RSC Sustainability

ROYAL SOCIETY OF CHEMISTRY

PAPER

View Article Online
View Journal

Cite this: DOI: 10.1039/d5su00924c

Large scale valorization of steel slag combined with membrane-based direct air capture for carbon mineralization: a techno-economic evaluation

Vitor Gama,†[a] Kyle Shank,†[b] Madison Morgan,[a] Owen Gerdes,[a] Savannah Sakhai,[a] Fernando V. Lima,[a] Shang Zhai *[bc] and Oishi Sanyal*[a]

The removal of carbon dioxide (CO_2) from the atmosphere and from hard-to-abate industrial processes such as steel production remains a significant challenge for meeting climate goals. Progressive studies on membrane-based direct air capture (m-DAC) have emerged to propose this technology as a promising option for addressing legacy emissions. Previous studies discussed computational techniques that can search for favorable operational regions and suitable membrane material properties that give satisfactory CO_2 capture performance and system energy efficiency. The combination of operability studies with membrane modeling and simulation represented a novel pathway to investigate fundamental material/process parameters tied to large-scale metrics. In this work, we explore a two-fold approach aiming to intensify CO_2 capture and utilization: (i) capturing CO_2 from ambient air (425 ppm) using m-DAC and concentrating it (25–50) times, and (ii) treating steel slags through CO_2 mineralization for the synthesis of cementitious materials. Each process was initially investigated separately, and their integration was then analyzed based on the overall technoeconomic viability and CO_2 removal efficiency per ton captured. The m-DAC process provides a low-purity (1–2%) CO_2 stream suitable for combination with mineralization. Slag-water CO_2 mineralization using 1% and 2% CO_2 achieves conversion rates of 55.4% and 43.3%, respectively, producing carbonated slag. Additionally, the slag can be reacted with steam to yield 16.99 std. ml H_2 per gram, utilizing waste heat from steelmaking. This dual process enables revenue generation from both H_2 production and carbonated slag, which can be sold as a supplementary cementitious material.

Received 17th December 2025
Accepted 8th April 2026

DOI: 10.1039/d5su00924c

rsc.li/rscsus

Sustainability spotlight

This work advances sustainable carbon management by integrating membrane-based direct air capture with the mineralization of CO_2 with steelmaking slag, transforming two environmental challenges into a unified climate solution. By permanently storing captured CO_2 in stable mineral products while valorizing industrial waste from steel production, the research promotes circular resource use and reduces emissions from hard-to-abate sectors. By coupling carbon removal with industrial waste valorization, this work promotes sustainable industrial innovation, supports resilient built environments, and contributes to long-term strategies for mitigating climate change. The techno-economic evaluation provides a clear pathway for scaling carbon capture and utilization technologies alongside renewable electricity.

1 Introduction

In March 2025, global atmospheric carbon dioxide levels reached an all-time high of 426.4 parts per million (ppm),[1] surpassing the previous year's record of 423.4 ppm.[3] This notable annual increase underscores the urgent demand to address the worldwide carbon dioxide crisis. To meet the goal of limiting the annual global temperature increase to 1.5 °C, emissions must be reduced by half by 2030, requiring the removal of tens of billions of metric tons of CO_2 within the coming years.[4] Thus development of scalable, economical and energy-efficient systems is critical to meet the net-zero target by 2050.[5] This target remains unachievable with existing technologies, as the largest operational direct air capture (DAC) facilities remove about 0.01 megatons of CO_2 per year.[6] At this time, technologies including Carbon Engineering's potassium hydroxide solvent system and Climeworks' solid-sorbent units remain in early commercial phases, with limited scalability.[7] Meanwhile, m-DAC systems remain at the laboratory, but offer a fundamentally different pathway for capturing CO_2 from

[a]Department of Chemical and Biomedical Engineering, West Virginia University, Morgantown, WV, USA. E-mail: oishi.sanyal@mail.wvu.edu
[b]Department of Mechanical and Aerospace Engineering, The Ohio State University, Columbus, OH, USA. E-mail: zhai.218@osu.edu
[c]School of Earth Sciences, The Ohio State University, Columbus, OH, USA
† These authors contributed equally to this work.

highly diluted air streams. Membranes may operate as standalone units or in hybrid configurations to selectively produce low-purity CO_2, making them well suited for air-based capture where conventional sorbent and solvent systems face scalability constraints.

This study presents a techno-economic analysis (TEA) of a combined CO_2 capture and utilization process. The capture process consists of an m-DAC configuration represented by hollow fiber membrane modules, in which the individual membranes operate *via* a facilitated transport mechanism, as demonstrated in the author's prior work.[2] The CO_2 mineralization process, on the other hand, uses steelmaking by-products to generate supplementary cementitious materials (SCMs), thereby locking CO_2 into a stable carbonate form. Membrane technologies offer several advantages in DAC applications, including modularity and operational flexibility.[8] Despite these benefits, current limitations include high estimated removal costs ranging from $3000 to $10 000 per ton of CO_2 captured for a small-scale two-stage process, which are not competitive with other commercial DAC technologies.[9] However, to the best of our knowledge, no DAC processes have yet reached the $100 per ton CO_2 target set by DOE.

The m-DAC system analyzed in this study was simulated using AVEVA Process Simulation, targeting outlet purities of 1% and 2% CO_2 for potential downstream applications including mineral carbonation or algae cultivation.[10]

To enhance the value proposition of m-DAC, this study examines a specific downstream CO_2 utilization strategy, with the integration of m-DAC capture with steel slag carbonation, to produce SCMs. These SCMs not only enable permanent mineralization of CO_2, but also improve the mechanical and hydraulic properties of construction-grade concrete.[11]

The mineralization pathway for producing SCMs is particularly attractive given the cement industry's high process emissions and significant material demand associated with ordinary Portland cement production. The production of ordinary Portland cement is a major source of CO_2 emissions, primarily due to the endothermic decomposition of limestone ($CaCO_3$) into lime (CaO) and CO_2, followed by the high temperature formation of calcium silicates – the main reactive components in cement.[12] Due to the energy and carbon intensity involved in both the calcination reaction and the calcium silicates formation reaction, there have been attempts to decrease cement usage by partially replacing it with SCMs.

Ground granulated blast furnace slag is a widely used SCM, whereas basic oxygen furnace (BOF) steel slag has limited SCM utilization due to low pozzolanic reactivity and the presence of expansive free CaO.[13] Carbonation of BOF slag converts free lime to a stable carbonate, mitigating expansion while permanently storing CO_2.

BOF slag carbonation has been investigated *via* gas–solid, direct aqueous, and indirect aqueous pathways.[13] Gas–solid routes typically require elevated pressures or temperatures, while indirect aqueous processes rely on additional chemical reagents, increasing cost.[14] Direct aqueous carbonation is therefore attractive, as it enables rapid CaO dissolution and CO_2 mineralization under mild conditions.

In addition, BOF slag contains reduced iron that can react with steam to produce hydrogen (H_2).[15] In this study, BOF slag is first used for H_2 generation through steam oxidation and then for CO_2 mineralization *via* a modified direct aqueous carbonation process.

In this work, we simulate a membrane-based DAC system that concentrates atmospheric CO_2 to 1–2% for slag-based CO_2 mineralization. We then experimentally assess the performance of these streams in a modified direct aqueous carbonation process using BOF steel slag following hydrogen generation. Finally, we integrate the capture and utilization pathways into a unified techno-economic analysis, evaluating capital costs under membrane and electricity zero-cost scenarios, and performing breakeven analyses based on product revenues. Together, these steps provide a comprehensive assessment of both the technical performance and economic feasibility of coupling facilitated-transport m-DAC with BOF-slag-based CO_2 mineralization for scalable and durable CO_2 removal.

2 Background

2.1 Gas transport in membranes

Gas permeation through membranes can occur by different mechanisms depending on the material characteristics and the presence of fixed or mobile carriers. In general terms, the flux of a gas component i is governed by the pressure difference across the selective layer and the intrinsic permeability of the material:

$$J_i = \frac{\mathscr{P}_i}{l} \times \left(p_{i,f} - p_{i,p}\right) \tag{1}$$

where $\mathscr{P}_i$ is the permeability of component i, $p_{i,f}$ and $p_{i,p}$ are its partial pressures on the feed and permeate sides, and l is the selective layer thickness.[9] When l is not precisely known, the property is commonly reported as permeance (P'), measured in gas permeation units (GPU):

$$P_i' = \frac{\mathscr{P}_i}{l} \tag{2}$$

2.1.1 Solution–diffusion membranes. The solution–diffusion (SD) mechanism describes transport through dense polymeric layers. It can be broken down into three sequential steps: adsorption of gas molecules at the upstream interface, molecular diffusion through the polymer matrix, and desorption at the downstream side. The permeability for SD membranes can be characterized by the product of component i diffusivity ($\mathscr{D}_i$) and solubility ($\mathscr{S}_i$):

$$\mathscr{P}_i = \mathscr{D}_i \times \mathscr{S}_i \tag{3}$$

and the corresponding flux is:

$$J_i^{\mathrm{SD}} = \frac{\left[\mathscr{D}_i \times \mathscr{S}_i\right]\left(p_{i,f} - p_{i,p}\right)}{l} \tag{4}$$

Although widely applied, SD membranes are limited by Robeson's upper bound, which highlights the trade-off between permeability and selectivity for polymer-based systems.[16,17]

2.1.2 Facilitated transport membranes. Facilitated transport (FT) membranes can overcome separation limitations since reactive carrier agents are incorporated into the selective layer. These carriers, typically amines or other functional moieties, can reversibly bind with CO_2 to form transient complexes. The reaction increases the effective solubility of CO_2, greatly enhancing its permeation relative to non-reactive gases such as N_2 and O_2, which continue to permeate by solution–diffusion alone.[18,19] The overall transport is thus a hybrid mechanism: at low CO_2 partial pressures, carrier-facilitated flux dominates; at higher pressures, carrier saturation causes a shift toward solution–diffusion. The total flux is expressed as:

$$J_{\text{total}} = J_{\text{SD}} + J_{\text{FT}} \tag{5}$$

where J_{SD} is given by eqn (4), and the facilitated transport term is:

$$J_{\text{FT}} = \frac{D_{\text{CO}_2}}{l} \times \left(\frac{K_{\text{eq.}} p_{\text{CO}_2,f}}{1 + K_{\text{eq.}} p_{\text{CO}_2,f}} - \frac{K_{\text{eq.}} p_{\text{CO}_2,p}}{1 + K_{\text{eq.}} p_{\text{CO}_2,p}} \right) \tag{6}$$

Here, D_{CO_2} represents a combined diffusivity–capacity parameter associated with the carrier sites concentration, and $K_{\text{eq.}}$ is the equilibrium constant for CO_2-carrier binding.[20] However, this mechanism does not represent the N_2 and O_2 transport since these molecules do not react with the carrier sites, ultimately following a solution diffusion flux only.

Compared to complex multi-parameter models, this framework represented by eqn (6), by Xu *et al.*[20] balances simplicity with physical accuracy. It enables direct regression of kinetic and thermodynamic parameters from experimental data. This makes it particularly useful for process-level modeling and performance prediction under varying feed conditions.[21]

It is important to note that facilitated-transport theory indicates that the separation performance is limited by coupled diffusion-reaction behavior, including carrier saturation and the existence of an optimal binding strength; increasing $K_{\text{eq.}}$ without bound does not monotonically increase facilitation and can introduce release/saturation limitations.[21] The aspirational values considered in this work are used as a bounding upper-limit case representative of a hypothetical high-carrier-density reactive membrane regime.

2.2 Background on cost estimation techniques

2.2.1 Classification of cost estimates. To ensure consistency in applying cost estimation methods to industrial processes, the Association for the Advancement of Cost Engineering (AACE International, 2016) provides a widely accepted classification framework, consolidated in Recommended Practice 18R-97. These guidelines define cost estimate classes, which encompass engineering, procurement, and construction practices (Table 1).

2.3 Equipment cost estimation models

When detailed project data are unavailable, equipment cost estimation models provide a practical approach to accelerate profitability evaluation. These models rely on correlations developed from empirical data, which link equipment cost to process characteristics such as throughput, phase of material (liquid, solid, or gas), or construction materials.[22,23]

2.3.1 Six-tenths rule. Among the available approaches, the capacity-exponent or "rule of thumb" method is one of the most widely applied in early stage studies, due to its simplicity and reasonable accuracy under data scarcity.[24] This rule estimates the cost of equipment using the equipment's capacity as parameter for cost estimation. When the exact cost is unavailable, eqn (7), relates the cost of two similar items with different capacities:

$$C_{\text{purch}} = C_{\text{ref}} \left(\frac{S}{S_{\text{ref}}} \right)^{n} \tag{7}$$

where: C_{purch} is the estimated purchase cost for size S (USD, base year). C_{ref} is a known cost at reference size S_{ref} (same base year and currency). n is the capacity exponent.

The value of n typically ranges from 0.5 to 0.85 depending on the equipment and plant type, with 0.6 being widely used in the chemical industry—hence the name six-tenths rule.[22,25] This equation captures the principle of economies of scale, in which larger equipment tends to cost less per unit capacity. While more detailed methods, such as vendor quotes or factorial approaches, may provide greater accuracy, the rule of thumb remains appropriate for preliminary screening studies such as the techno-economic evaluation proposed by this work.

2.3.2 Module costing technique. This method, considered one of the most reliable for preliminary cost estimation of new plants, begins with equipment base costs and adjusts them using correction factors for equipment type, operating pressure, and construction material.[23] The general formulation is as follows:

$$C_{\text{BM},i} = C_{\text{DE},i} + C_{\text{IDE},i} \tag{8}$$

$$C_{\text{DE},i} = C_{P0} + C_{\text{M}} + C_{\text{L}} \tag{9}$$

Table 1 Cost estimate classes and typical accuracy ranges (adapted from AACE International, 2016)

Class	Definition (%)	Accuracy range
5 – Order-of-magnitude	0–2	−50 to −20% (low); +30 to +100% (high)
4 – Study estimate	1–15	−30 to −15% (low); +20 to +50% (high)
3 – Budget/target	10–40	−20 to −10% (low); +10 to +30% (high)
2 – Control/engineering	30–70	−15 to −5% (low); +5 to +20% (high)
1 – Definitive/final	65–100	−3 to −1% (low); +3 to +15% (high)

$$C_{IDE,i} = C_{FIT} + C_O + C_E \quad (10)$$

Eqn (8) relates the bare module cost ($C_{BM,i}$) of equipment i to its direct and indirect costs.

- The direct costs (eqn (9)) include the base equipment cost (C_{P0}), material installation costs (C_M), and labor costs (C_L).
- The indirect costs (eqn (10)) account for freight, insurance, and taxes (C_{FIT}); overhead (C_O) such as vacation, retirement, and unemployment expenses; and engineering and project management services (C_E).

3 Methods

3.1 Membrane-based direct air capture (m-DAC) system

The TEA presented here builds on our previous work on facilitated transport membranes (FTMs) for direct air capture.[1,2] A single-stage membrane module was simulated to enrich CO_2 from ambient concentration (≈425 ppm) up to two different outlet conditions: 1 and 2% CO_2. While the base scenario, which considered the regressed intrinsic properties from ref. 20 of $K_{eq.} = 2.63 \times 10^{-5}$ Pa^{-1} and $D_{CO_2} = 3.79 \times 10^{-11} \times 10^{-8}$ mol m^{-1} s^{-1}, was able to achieve this target purity. However, the corresponding recovery was too low to justify cost evaluation. An NLP-based optimization framework was then applied to identify the property ranges that satisfied capture requirements of at least 50% recovery and CO_2 purity between 1–1.75%.[2] The optimal properties identified were $K_{eq.} = 4.04 \pm 1.23$ Pa^{-1} and $D_{CO_2} = 6.57 \times 10^{-8} \pm 2.44 \times 10^{-8}$ mol m^{-1} s^{-1}. These values are 4–5 orders of magnitude higher than the regressed base-case membrane properties obtained in the study by,[26] which employed the model suggested by.[20] Therefore, only scenarios with recoveries <50% are considered in the economic analysis. In Section 5 of the SI for this work, the limited recovery simulation is shown to demonstrate its poor performance, emphasizing that the baseline techno-economic scenario presented here is not commercially viable under current conditions. The results indicate that positive economic performance is only achieved under optimistic assumptions regarding the membrane properties assumed (Fig. 1).

3.1.1 Process description. The system consists of a hollow-fiber facilitated transport membrane operating under counter-current flow. Ambient air at 110 kPa flows through the shell side, while vacuum (2 kPa) is applied to the permeate side. The high pressure ratio (55) conditions enhances CO_2 flux and separation efficiency. Module specifications (fiber count, length, diameters, selective layer thickness) were based on previous research.[2]

The facilitated transport mechanism was modeled using eqn (6), where D_{CO_2} and $K_{eq.}$ represent the intrinsic membrane properties of diffusivity and binding constant.[20] Fig. 2 presents the process flow diagram (PFD) for the two CO_2 purities discussed.

3.1.2 Process simulation conditions and inverse design. The membrane separation process was simulated in AVEVA Process Simulation (APS) and more on different arrangements and operability studies can be found elsewhere.[1,2] D_{CO_2} and $K_{eq.}$ were regressed from experimental data, and the process simulation was used to train surrogate models to enable inverse mapping between desired outputs (purity, recovery) and intrinsic properties mentioned. Furthermore, in this study, the vacuum conditions were altered to obtain different purities in the permeate. This was performed seeking the best pairing conditions between the m-DAC CO_2 capture and the mineralization utilization. The simulated vacuum was set to 2 kPa in order to achieve CO_2 purities around 2% and adjusted to 4.5 kPa to reach 1%.

3.2 Mineralization process

3.2.1 Process description. In blast furnace-basic oxygen furnace (BF-BOF) steel production, iron ore (Fe^{3+} oxide) is first reduced to metallic iron (Fe) before being transferred to the BOF. In the BOF, oxygen is injected at high pressure to lower the

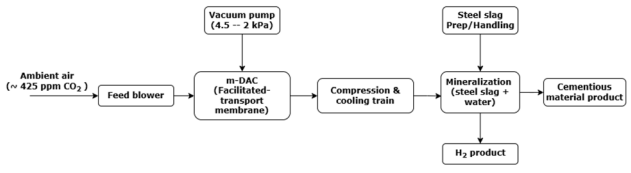

Fig. 1 Compact block flow of the integrated m-DAC and mineralization system. m-DAC enriches ambient air from 425 ppm to ≈1–2% CO_2; a three-stage compression train with interstage cooling conditions the stream for mineralization with steel slag, yielding a cement-like solid and H_2.

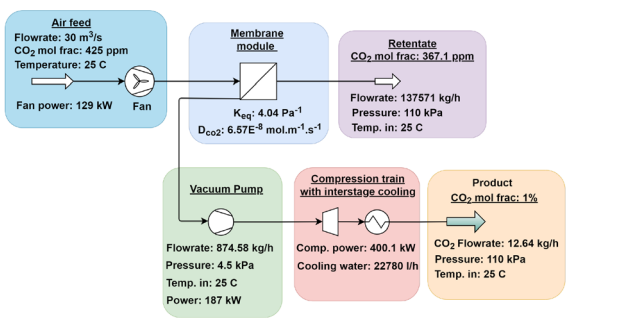

(a) Process PFD for 1% CO_2 permeate product

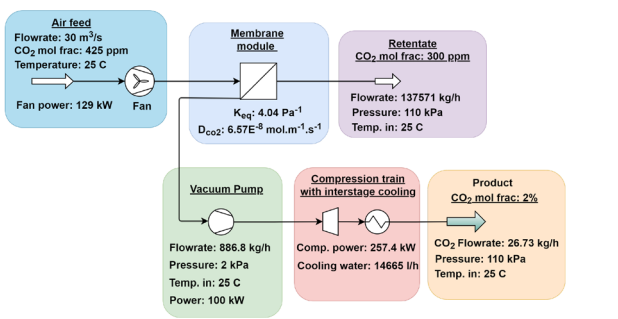

(b) Process PFD for 2% CO_2 permeate product

Fig. 2 m-DAC capture simulation PFD schemes. (a) 1% CO_2-permeante product arrangement. (b) 2% CO_2 permeate product arrangement.

carbon content of the melt. Fluxes are introduced during this stage to capture impurities, with CaO serving as the primary fluxing agent. CaO reacts with SiO_2 to produce calcium silicates—primarily Ca_2SiO_4 and Ca_3SiO_5—that rise to the surface of the melt as steel slag to be removed from the steel. Along with these silicates, some Fe^{2+} often gets incorporated into the steel slag. Our process begins with hydrogen (H_2) production through the reaction of steam with steel slag at 600 °C. As shown in eqn (11), residual Fe^{2+} in the slag exothermically reacts with water vapor to produce H_2 and Fe^{3+}. Water can be passed over hot slag, utilizing the residual heat from the BOF furnace to generate high-temperature steam. The resulting oxidized iron remains inert during the following hydration and mineralization reactions.

$$3FeO(s) + H_2O(g) \rightarrow Fe_3O_4(s) + H_2(g);\ \Delta H\ (600\ ^\circ C) = -55.72\ kJ\ mol^{-1} \quad (11)$$

After H_2 production, the steel slag is cooled and ground into a fine powder to serve as the feedstock for subsequent hydration and mineralization steps. During hydration, water reacts with the principal calcium-bearing phases in the slag—Ca_3SiO_5, Ca_2SiO_4, and CaO—as represented in (eqn (12)–(14)). Hydration of the calcium silicates yields calcium silicate hydrate ($3CaO{\cdot}2SiO_2{\cdot}8H_2O$, commonly referred to as CSH). The reaction pathways and corresponding heats of hydration for Ca_3SiO_5 and Ca_2SiO_4 are taken from the work of Mindess *et al.*[27]

$$2Ca_3SiO_5(s) + 11H_2O(l) \rightarrow 3CaO{\cdot}2SiO_2{\cdot}8H_2O(s) + 3Ca(OH)_2(aq.)\ \Delta H = -0.52\ kJ\ g_{Ca_3SiO_5}{}^{-1} \quad (12)$$

$$2Ca_2SiO_4(s) + 9H_2O(l) \rightarrow 3CaO{\cdot}2SiO_2{\cdot}8H_2O(s) + Ca(OH)_2(aq.)\ \Delta H = -0.26\ kJ\ g_{Ca_2SiO_4}{}^{-1} \quad (13)$$

$$CaO(s) + H_2O(l) \rightarrow Ca(OH)_2(aq.)\ \Delta H\ (45\ ^\circ C) = -84.2\ kJ\ mol^{-1} \quad (14)$$

Following hydration, the CSH and other solid components in the steel slag can be separated from the liquid phase. The remaining $Ca(OH)_2$ solution reacts with CO_2 to precipitate $CaCO_3$. Because only part of the water consumed in eqn (12)–(14) is regenerated in eqn (15), the overall process results in a net water deficit.

$$5CO_2(g) + 5Ca(OH)_2(aq.) \rightarrow 5CaCO_3(s) + 5H_2O(l)\ \Delta H\ (45\ ^\circ C) = -468.7\ kJ\ mol^{-1} \quad (15)$$

The precipitated $CaCO_3$ is then filtered from the liquid. At this stage, fresh steel slag and makeup water can be introduced, allowing the cycle to continue. The reaction enthalpies were calculated with data from Bale *et al.* (2002),[28] Bale *et al.* (2009)[29] and Reed.[30]

3.2.2 Process performance. In this section, a brief overview of the mineralization experiments, the resulting performance, and the scaled-up process description is provided. Detailed experimental procedures, along with the corresponding mass and energy balance methodologies, are presented in the SI.

Samples of BOF steel slag were sourced from Cleveland-Cliffs – Cleveland Works. The slag was collected directly from the BOF prior to the slagging-off process and was crushed into a fine powder for experimental testing. X-ray diffraction (XRD) analysis indicated that the slag was mostly composed of Ca_3SiO_5, Ca_2SiO_4, CaO, $Ca_2Fe_2O_5$, and $Mg_{0.8}Fe_{0.2}O$ (Fig. S1).

H_2 production performance was evaluated at 600 °C by flowing 100 sccm of 2% H_2O vapor in argon over 6 g slag. Under these conditions, the slag produced 16.99 std. ml H_2 per gram of slag (Fig. S2).

For mineralization, experiments were conducted using 1% and 2% CO_2/Ar mixtures, with water only blank runs performed for comparison. Each cycle used 0.5 g of slag with a 30 : 1 water-to-slag mass ratio. The experiments consisted of three cycles, each containing two sequential steps: hydration followed by CO_2 mineralization, with solid–liquid separation after each hydration step. During hydration, slag was reacted with water at 45 °C for 30 minutes. After separation, the mineralization step was carried out by flowing 40 sccm of either 1% or 2% CO_2 through the solution for 15 minutes, followed by a 20-minute argon purge to quantify the remaining CO_2 in the reactor. Fresh slag was added to the solution after the mineralization step. At the end of each hydration and mineralization step, the temperature and pH were measured. Fig. 3 presents the CO_2 mineralization results for 1% and 2% CO_2 feeds, showing 55.4% and 43.3% conversion respectively.

The mass and energy balance was initiated by scaling up the slag and water quantities proportionally to match the CO_2 flow rate produced by the DAC membrane system. The corresponding mass and energy balance of the mineralization system are summarized in Fig. 4 for 1% and 2% CO_2 cases, alongside the overall process schematic. All three reactions in the mineralization process are exothermic. Energy balances were performed for each reactor to evaluate the impact of reaction heat on reactor temperatures. From the net heat generated or removed over the reaction period and the heat capacity of the reactor contents, the resulting temperature change was estimated and

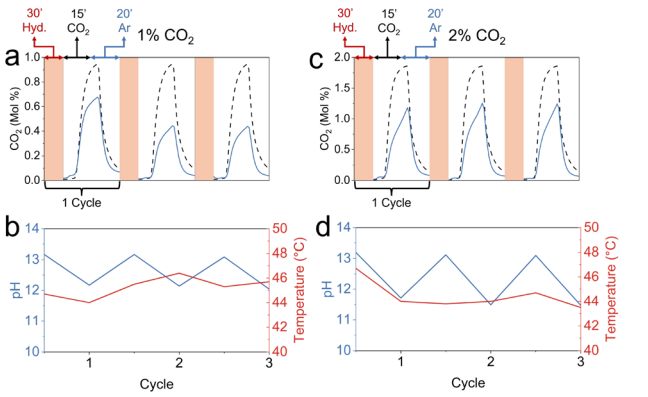

Fig. 3 (a) CO_2 mineralization with 1% CO_2. The black dashed line represents CO_2 inlet flow during a water-only blank run, while the solid blue line shows CO_2 outlet flow from the mineralization step. (b) Temperature and pH profile during 1% CO_2 mineralization. (c) CO_2 mineralization with 2% CO_2. (d) Temperature and pH profile during 2% CO_2 mineralization.

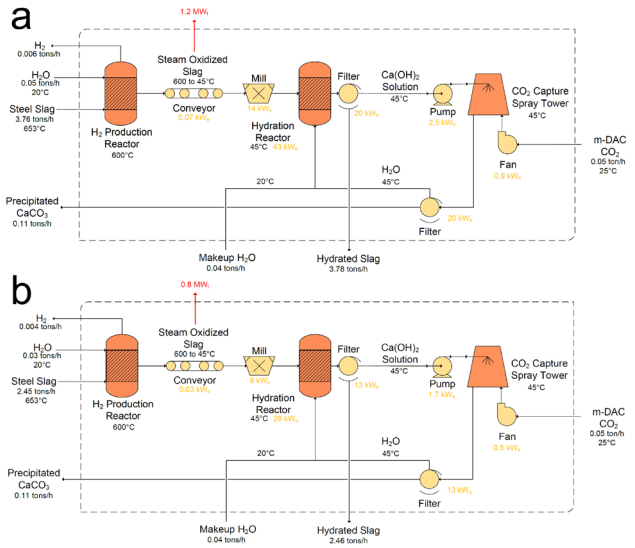

Fig. 4 CO_2 mineralization process diagrams for (a) 1% and (b) 2% CO_2.

found to be negligible (ΔT < 3 °C) for the H_2 production and hydration reactors. Similarly, for the CO_2 capture reactor, the liquid phase was assumed to remain at 45 °C, while the inlet gas stream at 25 °C removes reaction heat as it exits the system. Between the high-temperature H_2 production step and the low-temperature milling step prior to hydration, the slag cools from 600 °C to 45 °C during conveying. Since no internal process steps require additional thermal energy, this sensible heat was not recovered in the current analysis. In future process designs, the slag waste heat could potentially be utilized for low- to medium-grade heat applications, for example by coupling the cooling stage to a steam generator. Secondary unit operations such as milling, filtration, and pumping are assumed to operate isothermally at 45 °C.

3.3 Capital cost estimation

3.3.1 Equipment cost estimation. The major pieces of equipment involved in the combined process and the design parameter used for their cost estimation are noted in Table 2 below:

To estimate total fixed capital cost, the methodology developed by Towler, Gavin P., Sinnott, Ray K. (2021) was applied. Multipliers for installation, piping, control, and other items were included, leading to a factor of 6.0 on purchase cost for the m-DAC, since the CO_2 capture operation only handles gases, while the factor of 6.05 was used for the mineralization, since the latter involves both solids and gases.[22] Additionally, as noted in Section 3.2.2, the 1% permeate system required 4 units of membrane based capture, while 2% requires 5 units. Fig. 5 translate this difference in associated CAPEX for each CO_2 concentration considered. With that in mind, a multiplier for the total m-DAC cost was introduced to meet this objective based on the overall yield for each permeate condition, ultimately leading to the highest yield mineralization system to require less m-DAC units.

Table 2 Equipment list and capacity parameters used for cost estimation in the integrated m-DAC + mineralization system. Tables S1 and S2 in the SI provide additional details on the cost estimation parameters

Equipment	Capacity parameters	Units
m-DAC equipment		
Vacuum pump	Power	kW
Compressor	Power	kW
Heat exchanger	Heat-transfer area	m^2
Fan	Volumetric flow rate	$m^3\ s^{-1}$
Membrane module	Membrane area	m^2
Mineralization equipment		
Water splitting reactor	Reactor volume	m^3
Mill	Solids throughput	$Mg\ h^{-1}$
Hydration reactor	Reactor volume	m^3
CO_2 capture spray tower	Gas flow rate	$L\ s^{-1}$
Fan, centrifugal	Gas flow rate	$L\ s^{-1}$
Pump, centrifugal	Liquid flow rate	$L\ s^{-1}$
Rotary drum filter—slag	Filter area	m^2
Rotary drum filter—$CaCO_3$	Filter area	m^2
Conveyor	Vendor reference index[a]	$(Mg\ h^{-1})\ m^{2.5}$

[a] Vendor reference sizing (*e.g.*, solids capacity × length$^{2.5}$) used for quoting.

Using this method, the total fixed capital cost was estimated, considering 2015 as the base year (CEPCI = 556.8), and later updated using the CEPCI index for 2024 (CEPCI = 801.9) to correct the inflation effects.

3.3.2 Operating cost estimation. In this study, to improve transparency and reproducibility of the techno-economic analysis, the main economic assumptions used in the operating cost, revenue, net present value (NPV), and breakeven calculations are summarized in this section. Electricity cost was assumed to be \$0.06 kWh^{-1} and used as the baseline in all operating-cost calculations unless otherwise noted in the sensitivity analysis. Capital costs were estimated using the rule-of-thumb scaling approach described above and escalated to the analysis year using the CEPCI cost index. To represent policy-supported carbon removal revenue, the analysis includes the U.S. Section 45Q tax credit (a federal incentive for CO_2 capture and permanent storage). In this study, the 45Q credit is assumed to be \$100 per ton of CO_2 mineralized and stored in stable carbonate form, and is incorporated directly into the annual revenue calculations for both the 1% and 2% CO_2 feed cases.[31] Additional product revenues were calculated using an assumed hydrogen selling price of \$2 per kg and a carbonated slag selling price of \$26 per ton in the baseline TEA.[11,32] In the breakeven analysis (Section 4.4), the carbonated slag price was treated as the decision variable and back-calculated to determine the value required to achieve NPV = 0 over the project lifetime. The SI (Section 4) provides the equipment size parameters used in the rule-of-thumb cost estimation (corresponding to Table 2) to improve the reproducibility of the cost calculations.

For labor, a fixed staffing assumption was used for both process configurations. Specifically, five operators per shift were

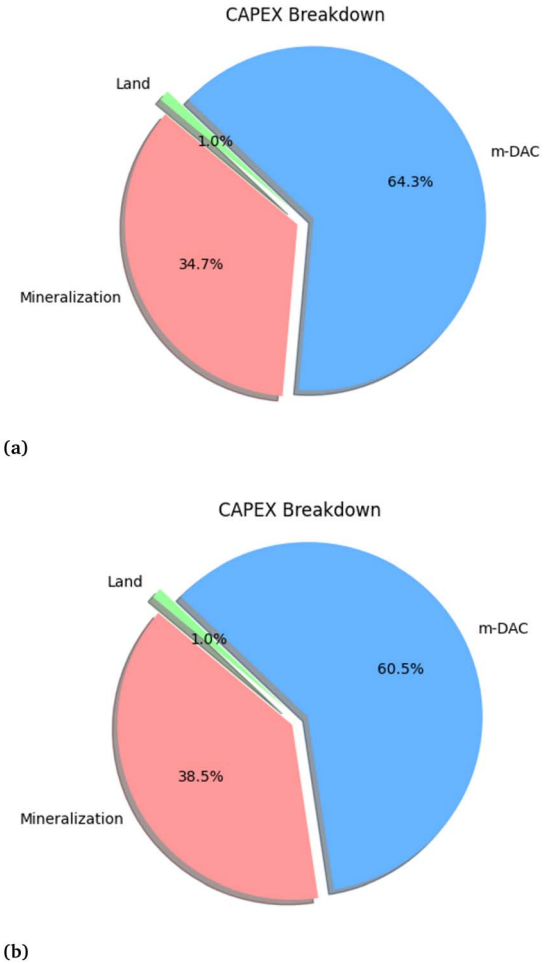

Fig. 5 CAPEX distribution comparison between (a) the case with 1% CO_2 purity in the m-DAC permeate stream and (b) the case with 2% CO_2 purity, both subsequently fed to the mineralization process. In both cases, CAPEX is dominated by the m-DAC unit, followed by mineralization, with land contributing a minor fraction.

assumed in total, including three operators for the m-DAC section and two operators for the mineralization section, with an annual wage of $63 210 per operator.[33] This corresponds to an annual labor cost of approximately $316 000 in both the 1% and 2% CO_2 feed cases. Therefore, the larger labor share reported in the 2% case reflects the lower total OPEX of that case, driven primarily by reduced electricity demand, rather than a substantial increase in absolute labor requirements.

3.3.3 Net present value (NPV). The economic feasibility of the project is evaluated using the Net Present Value (NPV) method, which measures the present worth of all future cash flows over an analysis horizon of n years (here, 45 years) discounted at a fixed rate r (10%). A 45-year plant life was assumed to reflect the intended co-location of the system with steel plants, whose long operational lifetimes (>40 years) and continued reinvestment support extended operation.[34–36] Let C_t represent the net cash flow in year t (revenues minus operating costs, taxes, *etc.*), with C_0 typically negative due to the initial capital investment (CAPEX). The NPV is given by:

$$\mathrm{NPV} = \sum_{t=0}^{n} \frac{C_t}{(1+r)^t} = -\mathrm{CAPEX}_0 + \sum_{t=1}^{n} \frac{\mathrm{Revenues}_t - \mathrm{OPEX}_t}{(1+r)^t} \tag{16}$$

A positive NPV (NPV > 0) indicates that discounted revenues exceed the total investment, making the project economically attractive, whereas NPV < 0 shows that revenues are insufficient to offset costs. The breakeven point occurs at NPV = 0, when discounted revenues exactly match capital and operating expenses and the internal rate of return equals the assumed discount rate. In addition to NPV, the breakeven analysis is used to determine when cumulative revenues offset total investment, using both simple (undiscounted) and discounted payback times. Together, these metrics provide a quantitative basis for evaluating long-term project viability under varying electricity prices, slag prices, and feed CO_2 conditions.

3.3.4 Annualized and levelized cost. To report costs on a yearly and per-ton basis, capital expenditures can be converted into an equivalent annual cost using the capital recovery factor (CRF). This approach spreads the total investment evenly over the analysis horizon considered by accounting for the time value of money through the discount rate r and the project lifetime n:

$$\mathrm{CRF}(r,n) = \frac{r(1+r)^n}{(1+r)^n - 1}, \quad \text{Annualized CAPEX} = \mathrm{CAPEX}_0 \cdot \mathrm{CRF}(r,n). \tag{17}$$

The total annualized cost is then given by:

$$\mathrm{Cost}_{\mathrm{annual}} = \text{Annualized CAPEX} + \overline{\mathrm{OPEX}}, \tag{18}$$

where $\overline{\mathrm{OPEX}}$ represents the average annual operating expenditure, including electricity, labor, maintenance, and other recurring costs. This approach can also compute any major component replacements or overhauls that may occur during the project lifetime, their future costs are discounted to present value and annualized using the same CRF formulation. Salvage values, if/when applicable, are discounted similarly and subtracted from the total capital cost. Annualizing costs enables consistent comparison among design alternatives that differ in scale or lifetime. This facilitates the calculation of levelized metrics (*e.g.*, cost per ton of CO_2 captured or mineralized), allowing direct evaluation of the influence of electricity price, slag price, and number of m-DAC units on the system's overall economic performance.

4 Results and discussion

4.1 Capital expenses

As the first step in the economic analysis of the capture, the process equipment estimated cost was calculated considering eqn (7), using the appropriate capacity factor required. It is important to note that the m-DAC capture and the mineralization had to be adapted for two different CO_2 concentrations—1% and 2%. In order to properly report the associated costs with

the process, all of the base purchase costs were assumed to have 2015 as reference year and consequently corrected to 2024. The productivity of a single m-DAC system has to be scaled-up by assuming parallel units to achieve the goal of removing at least 1000 tons of CO_2 per year, seeking to qualify for the 45Q tax credit. Prior to cost estimation, the APS flowsheets for the m-DAC system were optimized, focusing on reducing cooling-water demand in the compression train and adjusting heat-exchange duties to maintain equipment within safe operating limits.

Both cases show a similar CAPEX breakdown, with the major contribution attributed to the m-DAC units. This could be primarily attributed to the vacuum pumps and compressors used in the m-DAC process. Notably, the setup incorporating additional m-DAC units to offset reduced mineralization efficiency leads to a marginally lower overall CAPEX proportion for m-DAC (60.5% compared to 64.3%). This suggests that, from a capital investment standpoint, scaling up m-DAC may be more cost-effective than increasing the yield or throughput of the mineralization stage. This finding aligns with modularity-driven economies of scale: m-DAC units could often be scaled incrementally with relatively minor cost penalties, while mineralization systems may face nonlinear CAPEX growth due to solid handling, reactor sizing, or thermal integration constraints.

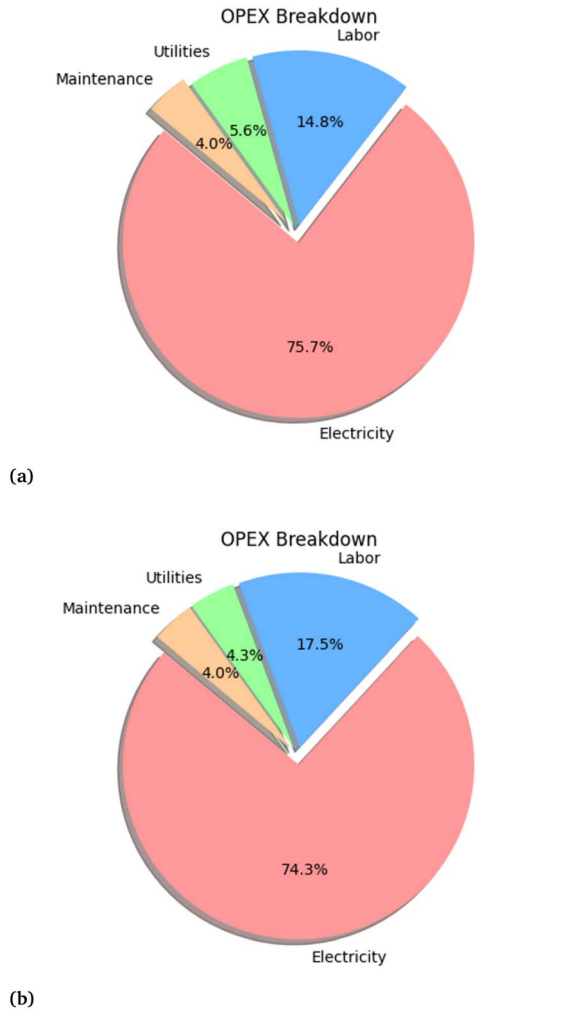

Fig. 6 OPEX distribution comparison between (a) the case with 1% CO_2 purity in the m-DAC permeate stream and (b) the case with 2% CO_2 purity, both subsequently fed to the mineralization process. In both cases, OPEX is dominated by electricity consumption, followed by labor, with utilities and maintenance contributing smaller shares.

4.2 Operational expenses

The operating expenditure (OPEX) shares for both cases, shown in Fig. 6, are dominated by electricity consumption, which accounts for over 74% of total OPEX in each case. Notably, the process with fewer m-DAC units and higher mineralization performance exhibits a slightly higher electricity share (75.7%) compared to the alternative case with more m-DAC units (74.3%).

This increase reflects the fact that the 1% case requires higher permeation across the membrane to meet the same capture target. The resulting higher permeate flow imposes a larger load on the compression train, increasing compressor power requirements and increasing the electricity share of the overall OPEX. However, because the labor expenses were treated as a fixed annual operating cost in both cases, its share of total OPEX increases in the 2% CO_2 case as the overall OPEX decreases, mainly due to lower electricity demand. Utility and maintenance costs remain relatively constant, indicating that the economic breakeven point mostly lies on energy consumption and product revenue. Overall, this comparison shows the delicate balance between modularity, and energy efficiency in capturing and mineralizing CO_2.

The advantage of coupling capture and utilization is discussed here to envision a scenario where a "carbon economy" drives investment to DAC and decarbonization processes through the 45Q tax credit. The revenue breakdown shown in Fig. 7 includes the U.S. 45Q tax credit, assumed at \$100 per ton of CO_2 permanently stored *via* mineralization. This value corresponds to the 45Q incentive level adopted in this study and is treated as a fixed revenue stream directly linked to the amount of CO_2 mineralized. In addition, product revenues are calculated using a hydrogen selling price of \$2 per kg and a carbonated slag selling price of \$26 per ton. These values are held constant in the baseline NPV analysis; only the carbonated slag price is varied in the breakeven analysis (Section 4.4), where it is back-calculated to determine the price required to achieve NPV = 0 over the project lifetime. Additionally, during the carbonation of the steel slag, besides the carbonated slag, hydrogen is generated as a byproduct which fortunately can also be sold, adding value to the combined process. In addition to these direct revenue streams, utilizing BOF steel slag offers an implicit economic advantage by avoiding disposal and handling costs. Steel slag is often sent to landfills due to its limited reactivity, creating long-term management burdens for steel producers. Although these avoided costs were not explicitly quantified in this TEA, they represent a meaningful indirect economic benefit that could further improve the viability of the integrated m-DAC and mineralization process.

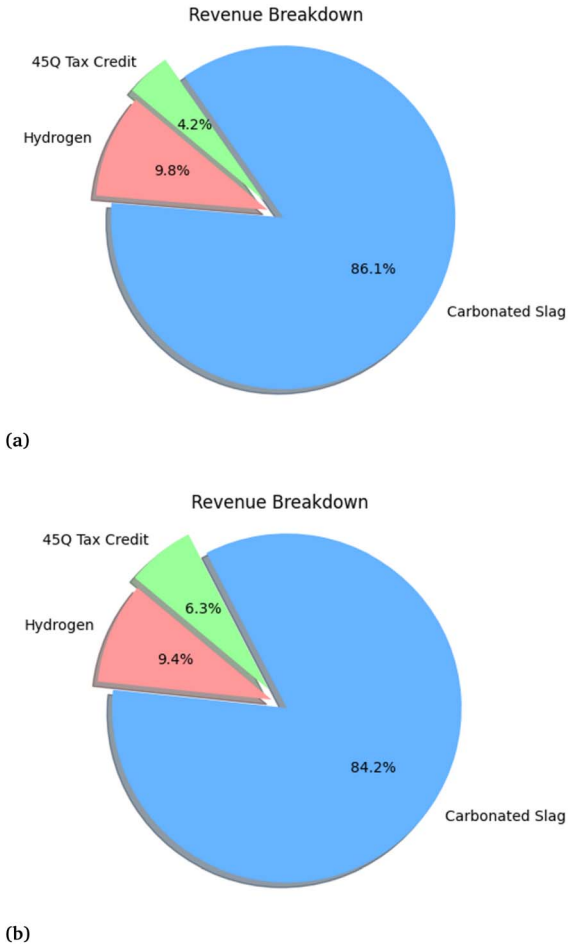

Fig. 7 Revenue distribution comparison between (a) the case with 1% CO_2 purity in the m-DAC permeate stream and (b) the case with 2% CO_2 purity, both subsequently fed to the mineralization process. In both cases, revenue is dominated by carbonated slag sales, followed by hydrogen, with the 45Q tax credit contributing a smaller share.

4.3 NPV analysis

In the 1% case, the analysis spans a 45-year operational horizon with a 10% discount rate. Although a 10% discount rate is typically associated with shorter economic evaluations, it was held constant here due to the early-stage nature of m-DAC and the lack of established discounting practices for long-term DAC infrastructure.

Maintaining a fixed rate provides a consistent baseline for comparison while acknowledging the uncertainty surrounding appropriate risk-adjusted rates for emerging carbon-removal technologies. The key TEA results for this case are:

- Initial CAPEX: −$57.5 million
- Annual revenue: $2.33 million
- Annual OPEX: −$2.14 million
- Annual profit (undiscounted): $188 000
- Resulting NPV: −$55.6 million
- Payback time: over 300 years (unrealistic within project lifetime)
- Discounted breakeven: not reached within 45 years

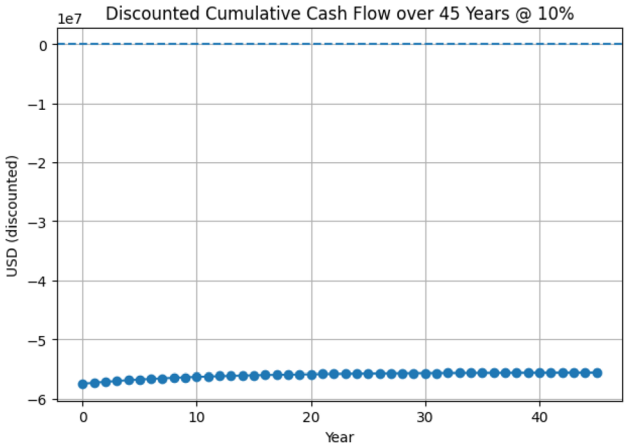

Fig. 8 NPV profile for the 1% CO_2 feed case, based on discounted cash-flow analysis using CO_2 permeate from the m-DAC capture unit as the feed to the mineralization step.

The NPV plot, in Fig. 8, confirms the above outcomes, showing a flat, negative trend throughout the plant's life. Despite modest annual profits, the magnitude of the CAPEX investment vastly outweighs the cumulative returns. Importantly, the NPV does not show a trend toward zero at any point, which implies that under current economic and technical assumptions, this configuration is fundamentally nonviable from a financial standpoint. This result suggests that improvements in revenue generation (*e.g.*, product pricing or carbon credit incentives) or cost reduction (especially CAPEX) would be essential to make this design attractive.

In contrast to the 1% scenario, the 2% configuration has a reduced capital expenditure but fails to achieve any positive yearly profit, resulting in a slightly less negative but still unfavorable NPV.

Key results include:

- Initial CAPEX: −$40.3 million, about 30% lower than the 1% case.
- Annual revenue: $1.50 million, substantially reduced due to lower mineralization performance and possibly lower throughput.
- Annual OPEX: −$1.81 million, moderately lower than in the 1% case.
- Annual profit: negative at −$302 000, meaning the plant operates at a net annual loss.
- NPV @ 10%: −$43.3 million
- Simple payback: not applicable, due to no profitable years.
- Discounted breakeven: not reached within the 45-year horizon

The cash flow plot further confirms the poor economic outcome: the cumulative discounted cash flow declines continuously, although with a lower slope compared to the 1% case. This reflects lower upfront investment and operating costs, but the inability to cover them due to insufficient revenue generation. Although the 2% case benefits from a lower capital cost, the drop in revenue and the shift from marginal profit to annual losses results in a project that is still economically

unattractive. This result highlights a critical insight: lower CAPEX does not guarantee better economic performance if operational revenues decline disproportionately, particularly when fixed OPEX and depreciation continue to apply. For both configurations, the root issue is insufficient annual cash flow to justify the scale of investment. It should be further noted that the m-DAC simulations considered membrane material properties such as D_{CO_2} and $K_{eq.}$ to be 4–5 orders of magnitude times higher than the values regressed from pior literature. Therefore, these values are already aspirational, and further improvements in their magnitudes cannot be expected.

When comparing the discounted cumulative cash-flow trend for the 1% and 2% feed cases, the key difference in their shapes arises from the sign of the annual operating profit. In the 1% configuration, annual revenue ($2.33 million) marginally exceeds annual OPEX ($−2.14 million), yielding a small positive yearly profit of approximately $188 000. Even after discounting, this positive rate contributes to slight incremental gains each year, producing the small upward drift observed in the cumulative discounted cash flow curve, although the magnitude of the annual profit is far too small to offset the large initial CAPEX. In contrast, the 2% case operates at an annual loss, as revenue ($1.50 million) falls below OPEX ($−1.81 million), resulting in a negative yearly profit of −$302 000. Consequently, each operational year adds a discounted deficit rather than a surplus, causing the cumulative cash flow to decline steadily over the 45-year horizon.

It is important to note that a direct comparison between the present m-DAC system and conventional DAC technologies is not strictly equivalent. Most large-scale DAC projects are designed to produce high-purity CO_2 streams (95–99%), which are suitable for compression and geological storage, with reported capture costs in the range of $600–900 per ton CO_2 removed (*e.g.*, McQueen *et al.*[37]). In contrast, the present system is intentionally designed to deliver a low-purity (1–2%) CO_2 stream for direct downstream mineralization. Since separation cost strongly depends on the target purity and pressure specifications, comparing a 1–2% product to a 95–99% product would not reflect equivalent system objectives.

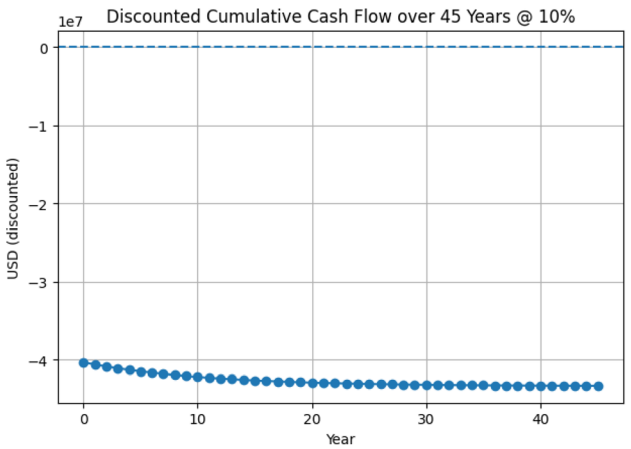

Fig. 9 NPV profile for the 2% CO_2 feed case, based on discounted cash-flow analysis using CO_2 permeate from the m-DAC capture unit as the feed to the mineralization step.

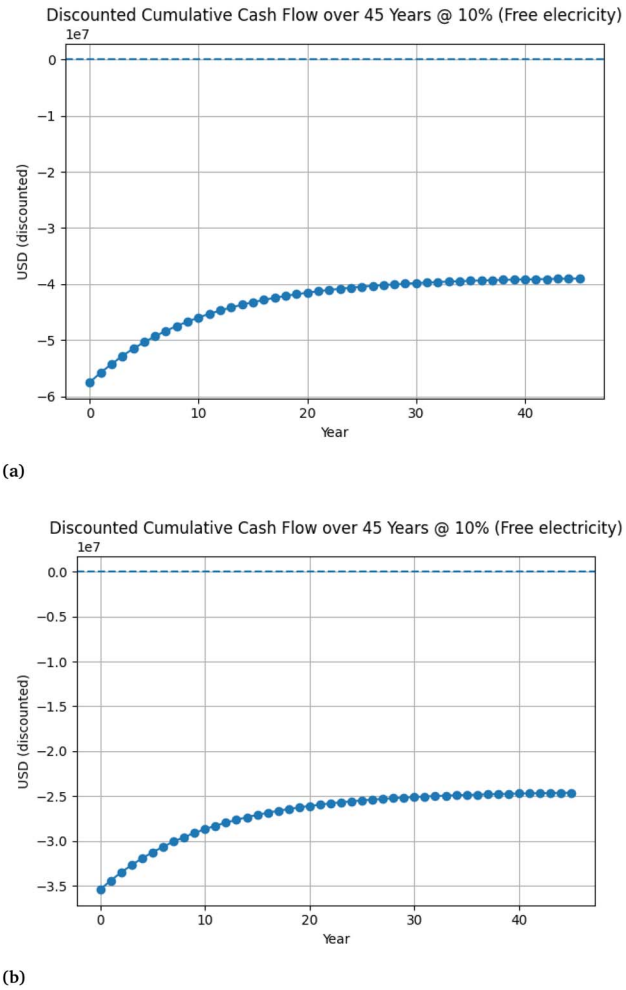

Fig. 10 Discounted cumulative cash flow comparison over 45 years at a 10% discount rate between (a) the case with 1% CO_2 purity in the m-DAC permeate stream and (b) the case with 2% CO_2 purity, both subsequently fed to the mineralization process, under a free electricity cost scenario. In both cases, the cumulative cash flow remains negative throughout the analysis period, indicating that eliminating electricity costs alone is insufficient to achieve economic viability.

4.4 Breakeven analysis

Given the high capital and operating expenditures associated with m-DAC and mineralization processes, additional NPV calculations were conducted to assess the economic sensitivity of the system to two critical parameters: membrane capital cost and electricity price. These parameters were selected due to their influence on the capital (membranes) and operating (electricity) sides of the techno-economic analysis, as shown in the CAPEX/OPEX breakdowns in Fig. 5 and 6 and NPV evaluations in Fig. 8 and 9. To isolate the role of electricity cost, the NPV profiles of both configurations were recalculated assuming free electricity, effectively removing the dominant OPEX component (previously ≈75%).

Table 3 NPV comparison under cost reduction scenarios

Scenario	1% CO_2 feed case	2% CO_2 feed case	Impact
Free electricity	Moderate recovery but still negative	Slope reduction, smaller NPV loss	High
Free membrane	Minor improvement, near-flat trend	Slightly smaller initial loss	Low

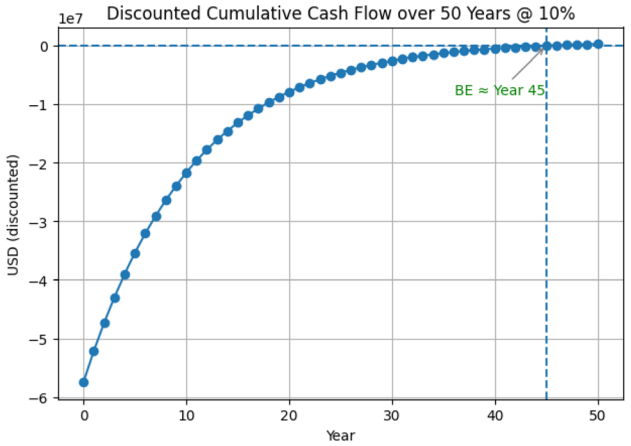

Fig. 11 Discounted cumulative cash flow for the 1% CO_2 feed case at a 10% discount rate. At a carbonated slag price of $99.26 per ton, breakeven is only achieved near the end of the 50-year project lifetime (Year ≈ 45).

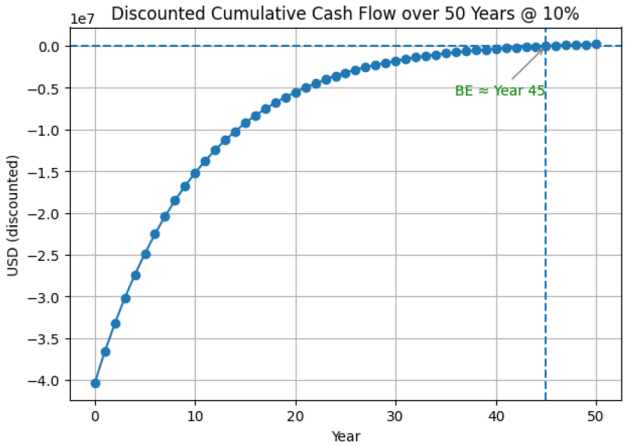

Fig. 12 Discounted cumulative cash flow for the 2% CO_2 feed case over 50 years at 10% discount rate, assuming a slag selling price of $116.17 per ton. Breakeven occurs at year 45.

In the 1% case, Fig. 10(a), the removal of electricity cost significantly flattens the cash flow trajectory but does not enable breakeven within the 45-year window. The NPV remains negative, though the magnitude of the loss decreases. In the 2% case, Fig. 10(b), the reduced OPEX from free electricity improves performance similarly. The NPV becomes less negative, indicating partial mitigation of financial losses. This scenario demonstrates that electricity price is a critical limiting factor, but not the sole barrier to economic viability. Even in the absence of energy costs, the high CAPEX and low revenue (especially from carbonated slag) continue to hinder positive returns. The next analysis explores the impact of eliminating membrane CAPEX, simulating a best-case scenario where membrane technology becomes low-cost or is subsidized. When combined with the previously analyzed free electricity scenario, this will help identify whether current unprofitability is primarily driven by capital intensity, energy dependence, or insufficient revenue streams. The discounted cumulative cash flow plots for both 1% and 2% scenarios under the free membrane cost assumption provide a sharp contrast with the earlier free electricity cases (Table 3):

With this framing in place, understanding the important role of electricity in cost and disregarding the influence of the membrane impact, the slag price will be assessed seeking to find a breakeven point by determining the minimum slag selling price that would make either case (or both) financially viable. To identify the market conditions under which the process may become economically viable, a breakeven analysis was conducted by adjusting the selling price of the carbonated slag product while keeping all other parameters constant. This approach directly addresses the revenue deficit observed in the baseline NPV analysis.

The breakeven analyses for both scenarios were designed by setting the project lifetime (45 years) as a parameter and adjusting the carbonated slag selling price to ensure economic viability within that time frame. This approach provides insight into the minimum viable product price necessary to recover investment and achieve a NPV = 0 under a fixed operational horizon and discount rate. For the 1% CO_2 use case, a slag price of $99.26 per ton enables breakeven exactly at year 45 (Fig. 11). This value was selected to remain under the $100 per ton threshold, reflecting a potential upper limit for market feasibility in commodity applications. The curve shows a consistent rise in cumulative value with time, driven by positive annual cash flows, but the expressive CAPEX at year 0 underscores the barrier for profitability. This extended payback period, combined with the relatively high product price needed, suggests that the economic viability of this configuration is highly sensitive to slag market conditions.

A similar breakeven analysis was performed for the 2% CO_2 use configuration by adjusting the slag selling price such that cumulative discounted cash flows reach zero by year 45. As

Table 4 Cost summary for 1% and 2% CO_2 feed cases (45-year amortization). All costs are reported in $ per ton of captured CO_2

Cost category	1% feed	2% feed
Overall capture & mineralization	$8203	$6225
Overall capture only	$3221	$1868

Table 5 Annual CO_2 balance (grid electricity[a]: 0.000367 ton CO_2 emitted per kWh)

	1% feed	2% feed
Total CO_2 emitted [ton per year]	2994.10	1958.92
Total CO_2 captured [ton per year]	970.96	947.17
Net CO_2 emissions [ton per year]	2023.14	1011.75

[a] Renewable sources represent a share of 40% (including nuclear power sources) of the total U.S. grid power generation.

Table 6 Annual CO_2 balance (100% renewable sources: 0.00003075 ton CO_2 emitted per kWh)

	1% feed	2% feed
Total CO_2 emitted [ton per year]	250.87	164.13
Total CO_2 captured [ton per year]	970.96	947.17
Net CO_2 emissions [ton per year]	−720.09	−783.04

Table 7 Annual CO_2 balance (25/75 grid/renewable sources: 0.0001148125 ton CO_2 emitted per kWh)

	1% feed	2% feed
Total CO_2 emitted [ton per year]	961.76	702.57
Total CO_2 captured [ton per year]	970.96	947.17
Net CO_2 emissions [ton per year]	−34.28	−65.13

shown in Fig. 12, a slag price of \$116.17 per metric ton is required for the process to achieve breakeven precisely at the end of the 45-year operational period. Compared to the 1% case, the required slag price is higher by approximately \$17 per ton. This increase can be attributed to the greater capital and operational costs of the 2% CO_2 permeate design, which includes one additional m-DAC unit. The presence of this extra unit increases not only the initial investment but also the recurring OPEX, particularly in terms of electricity and labor, as previously noted in the OPEX breakdown. Notably, in both cases, the breakeven was not an unknown variable in the TEA, but rather a targeted constraint used to back-calculate the necessary revenue (*via* slag pricing). This allowed us to precisely identify a critical threshold for the carbonated slag and ultimately inform market development efforts and policy actions. Table 4 summarizes the TEA analysis comparing the levelized costs per ton of CO_2 that ultimately is mineralized and the cost considering just capture without utilization.

4.5 Emissions impact

The carbon intensity of the capture process was evaluated by coupling the m-DAC and mineralization systems with different electricity supply scenarios, ranging from fully powered by the US grid to fully renewable energy and mixed configurations. While grid-powered operation results in net-positive emissions due to the high carbon footprint of conventional electricity generation, progressively increasing the renewable share leads to a clear reduction in total emissions. At high renewable fractions, both 1% and 2% feed cases achieve net-negative operation, with the 2% feed configuration consistently showing greater CO_2 removal owing to its higher process efficiency and improved mineralization performance.

With grid power, both cases are net positive emitters because electricity-related emissions dominate the carbon balance.

Under 100% renewables, both systems become net negative; the 2% feed removes slightly more CO_2 overall (Table 7).

With a 75% renewable share, both configurations achieve net-negative emissions, with deeper removal for the 2% feed.

5 Conclusions

The techno-economic evaluation indicates that the viability of this process remains strongly dependent on its integration with a downstream utilization pathway. When considered by itself, the capture step alone exhibits prohibitively high costs—reaching \$3221.33 and \$1868.03 per ton of CO_2 for the 1% and 2% CO_2 permeates, respectively (Table 4). These costs are well above current benchmarks for DAC technologies, confirming that membranes, though promising for continuous modular operation, require strong economic incentives and/or a revenue-generating utilization process to be competitive.

When capture is coupled with carbonated slag production, the cost per ton of CO_2 utilized are \$8203.05 and \$6224.62 for the 1% and 2% CO_2 feed conditions, respectively. Despite proposing a new pathway to associate capture and utilization of CO_2, the overall process remains capital-intensive, with initial investments dominated by the m-DAC subsystem (approximately 60–65% of total CAPEX; Fig. 5), mostly due to the multiple number of m-DAC units required. Furthermore, electricity contributes over 74% of OPEX (Fig. 6), emphasizing that operational viability hinges on the availability of low-cost, low-carbon power. This relationship was further seen by the free-electricity sensitivity tests, which showed that even complete removal of energy costs could not ensure a positive NPV within a 45-year lifetime. Hence, the energy intensity of the process is found to be the main bottleneck, followed by limited product revenue.

A key implication of this bottleneck is that m-DAC is unlikely to become competitive through bulk air compression alone. Prior m-DAC studies have shown that, because atmospheric CO_2 is extremely dilute, the main technical challenge is generating sufficient transmembrane driving force without surpassing prohibitive power demands. In this context, permeate-side vacuum is generally more energy-favorable than feed compression, although it also increases membrane-area requirements and places greater importance on low pressure-drop module design.[9,38,39] At the materials level, the literature further indicates that progress will depend not only on increasing intrinsic CO_2/N_2 selectivity and CO_2 permeance, but also on translating these properties into scalable ultra-thin asymmetric or facilitated-transport membranes that retain performance under humid, oxygen-containing DAC conditions while resisting physical aging, swelling, and carrier instability. Thus, the most credible pathway forward is a lower-energy m-DAC system in which membranes operate as modular pre-concentration units. This system would be supported by

vacuum- or sweep-assisted operation and low pressure-drop contactors. It would also rely on hybrid integration with downstream mineralization or other utilization steps that can handle intermediate purity CO_2 streams, rather than requiring high purity CO_2 at the capture stage.

The breakeven analyses also reinforce these findings. For the process to achieve economic neutrality within the project lifetime (45 years), the carbonated slag must be sold at \$99.26 per ton for the 1% configuration and \$116.17 per ton for the 2% configuration (Fig. 11 and 12). These prices are three to five times higher than the projected market value of carbonated steel slag (\$20–\$30 per ton) and exceed the selling price of ground granulated blast furnace slags (GGBFS) ($\approx$50 \$ per ton). This suggests that the process would only be profitable if the carbonated slag can be further refined as a SCM or as a material that can qualify for carbon credit incentives.

From an environmental standpoint, the system's carbon emissions exhibited a high correlation to the electricity source. When fully powered by the current U.S. grid mix, both configurations act as net emitters, releasing 2023 and 1012 tons of CO_2 per year for the 1% and 2% cases, respectively (Table 5). Transitioning to renewable energy drastically shifts the outcome, achieving net-negative emissions of up to -720 and -783 tons CO_2 per year under 100% renewable supply (Table 6). Even partial renewable integration (*e.g.*, 75% renewable) yields small but measurable net removal, confirming that decarbonizing the electricity supply is a prerequisite for this technology to contribute effectively to negative emissions targets.

Overall, this study shows that although membrane-based DAC paired with BOF steel-slag mineralization can technically deliver continuous carbon capture and sequestration, its economic feasibility hinges on favorable market and policy conditions; particularly scenarios that combine low-carbon electricity, lower membrane and compression costs, and effective valorization of both carbonated slag and hydrogen byproducts. Under these conditions, and with continued progress in renewable-energy integration and material upgrading, the proposed hybrid process could become a scalable, regionally deployable pathway for permanent CO_2 removal.

Conflicts of interest

There are no conflicts to declare.

Data availability

Data supporting this publication are available from the corresponding author upon reasonable request.

Supplementary information (SI): additional experimental, modeling, and techno-economic details supporting the analysis presented in the main text; CO_2 mineralization reaction data and procedures, mass and energy balance calculations, supplementary m-DAC simulation discussions, and detailed equipment sizing parameters used for cost estimation to support transparency and reproducibility. See DOI: https://doi.org/10.1039/d5su00924c.

Acknowledgements

V. G., F. V. L. and O. S. acknowledge funding from NSF RII Track-2 FEC (OIA-2119688) and NASA Established Program to Stimulate Competitive Research through Grant #80NSSC22M0027. K. S. and S. Z. acknowledge support from the Sustainability Research Seed Grant at The Ohio State University. The authors thank Cleveland-Cliffs – Cleveland Works for providing steel slag samples. Support from the Center for Electron Microscopy and Analysis (CEMAS) at The Ohio State University is gratefully acknowledged. K. S. is supported by the Distinguished University Fellowship and the ENGIE-Axium Fellowship at The Ohio State University.

Notes and references

1 V. Gama, B. Dantas, O. Sanyal and F. V. Lima, *ACS Eng. Au*, 2024, **4**, 394–404.
2 V. Gama, D. Roy, F. V. Lima and O. Sanyal, *Ind. Eng. Chem. Res.*, 2025, **64**, 8375–8389.
3 Global Monitoring Laboratory, *Trends in CO_2*, NOAA Global Monitoring Laboratory, 2025, https://gml.noaa.gov/ccgg/trends/monthly.html, accessed on: 2025-08-07.
4 U. Nations, Goal 13: Take urgent action to combat climate change and its impacts, 2025, https://www.un.org/sustainabledevelopment/climate-change/.
5 U. Nations, *Net Zero Coalition*, Publisher, United Nations, 2025, https://www.un.org/en/climatechange/net-zero-coalition, accessed 7 August 2025.
6 Direct Air Capture – Energy System, 2025, https://www.iea.org/energy-system/carbon-capture-utilisation-and-storage/direct-air-capture.
7 EFI Foundation, Direct Air Capture: The Rapidly Expanding Landscape – From Kiloton to Megaton Scale, 2025, https://efifoundation.org/foundation-reports/annual-report-2024/.
8 Y. Jia, K. Wong, C. Z. Liang, J. Wu, T.-S. Chung and S. Zhang, *Prog. Mater. Sci.*, 2024, **146**, 101324.
9 C. Castel, R. Bounaceur and E. Favre, *Front. Chem. Eng.*, 2021, **3**, 668867.
10 H. Leflay, J. Pandhal and S. Brown, *J. CO_2 Util.*, 2021, **52**, 101657.
11 Q. Song, M.-Z. Guo, M. Zhang and T.-C. Ling, *J. Clean. Prod.*, 2024, **469**, 143214.
12 T. Hottle, T. R. Hawkins, C. Chiquelin, B. Lange, B. Young, P. Sun, A. Elgowainy and M. Wang, *J. Clean. Prod.*, 2022, **363**, 131834.
13 Y. Zhang, L. Yu, K. Cui, H. Wang and T. Fu, *Chem. Eng. J.*, 2023, **455**, 140552.
14 Y. Wang, J. Liu, X. Hu, J. Chang, T. Zhang and C. Shi, *J. Sustainable Cem.-Based Mater.*, 2023, **12**, 471–486.
15 P. Li, Y. Chen, X. Li, B. Yan, D. Chen and H. Guo, *Int. J. Hydrogen Energy*, 2020, **45**, 17140–17152.
16 L. M. Robeson, *J. Membr. Sci.*, 2008, **320**, 390–400.
17 R. Sidhikku Kandath Valappil, N. Ghasem and M. Al-Marzouqi, *J. Ind. Eng. Chem.*, 2021, **98**, 103–129.
18 Y. Chen, L. Zhao, B. Wang, P. Dutta and W. Winston Ho, *J. Membr. Sci.*, 2016, **497**, 21–28.

19 Z. Tong and W. S. W. Ho, *Sep. Sci. Technol.*, 2017, **52**, 156–167.
20 H. Xu, S. G. Pate and C. P. O'Brien, *Chem. Eng. J.*, 2023, **460**, 141728.
21 R. Rea, M. De Angelis and M. Baschetti, *Membranes*, 2019, **9**, 26.
22 G. P. Towler and R. K. Sinnott, *Chemical Engineering Design : Principles, Practice and Economics of Plant and Process Design*, Butterworth-Heinemann, 2nd edn, 2021.
23 *Analysis, Synthesis, and Design of Chemical Processes*, ed. R. Turton, Prentice Hall, Boston, 5th edn, 2018.
24 D. R. Woods, *Rules of Thumb in Engineering Practice*, Wiley, 1st edn, 2007.
25 S. Lemmens, *Energies*, 2016, **9**, 485.
26 Y.-Y. Lee, N. P. Wickramasinghe, R. Dikki, D. L. Jan and B. Gurkan, *Nanoscale*, 2022, **14**, 12638–12650.
27 S. Mindess, J. F. Young and D. Darwin, *Concrete*, Prentice Hall, 2nd edn, 2003.
28 C. Bale, P. Chartrand, S. Degterov, G. Eriksson, K. Hack, R. Ben Mahfoud, J. Melançon, A. Pelton and S. Petersen, *Calphad*, 2002, **26**, 189–228.
29 C. Bale, E. Bélisle, P. Chartrand, S. Decterov, G. Eriksson, K. Hack, I.-H. Jung, Y.-B. Kang, J. Melançon, A. Pelton, C. Robelin and S. Petersen, *Calphad*, 2009, **33**, 295–311.
30 J. J. Reed, The NBS Tables of Chemical Thermodynamic Properties: Selected Values for Inorganic and C1 and C2 Organic Substances in SI Units, 1989, https://data.nist.gov/od/id/mds2-2124.
31 45Q Tax Credit for Carbon Capture Projects. Carbon Capture Coalition, https://carboncapturecoalition.org/resource/45q-tax-credit-for-carbon-capture-projects/, accessed on: 2026-03-11.
32 Hydrogen Production. Energy.gov, https://www.energy.gov/eere/fuelcells/hydrogen-production, acessed on: 2026-03-17.
33 Chemical Equipment Operators and Tenders. Bureau of Labor Statistics, https://www.bls.gov/oes/2023/may/oes519011.htm, acessed on: 2026-03-11.
34 U.S. Energy Information Administration, *Energy Implications of Potential Iron and Steel-Sector Decarbonization Pathways*, U.S. Department of Energy, ieo2021 issues in focus, 2022.
35 K. Shank, H. Xu, Y. Xu, A. A. Kermani, J. Qin and S. Zhai, *Energy Environ. Sci.*, 2026, **19**, 2194–2212.
36 N. Badger, R. Boylu, V. Ilojianya, M. Erguvan and S. Amini, *Energy Adv.*, 2024, **3**, 2311–2327.
37 N. McQueen, K. V. Gomes, C. McCormick, K. Blumanthal, M. Pisciotta and J. Wilcox, *Prog. Energy*, 2021, **3**, 032001.
38 S. Fujikawa, R. Selyanchyn and T. Kunitake, *Polym. J.*, 2021, **53**, 111–119.
39 P. Panja, C. Manankandayalage, M. M. Alam and M. Deo, *J. Appl. Polym. Sci.*, 2023, e54802.